Draft version October 21, 2008
Preprint typeset using LaTeX style emulateapj v. 11/26/04

arXiv:0807.4949v2 [astro-ph] 17 Oct 2008

BH ACCRETION IN LOW-MASS GALAXIES SINCE $Z \sim 1$

Yong Shi[1], George Rieke[1], Jennifer Donley[1], Michael Cooper[1,7], Christopher Willmer[1], Evan Kirby[4]

Draft version October 21, 2008

ABSTRACT

We have selected a sample of X-ray-emitting active galactic nuclei (AGNs) in low-mass host galaxies (~5×10^9- 2×10^{10} $M_\odot$) out to z~1. By comparing to AGNs in more massive hosts, we have found that the AGN spatial number density and the fraction of galaxies hosting AGNs depends strongly on the host mass, with the AGN host mass function peaking at intermediate mass and with the AGN fraction increasing with host mass. AGNs in low-mass hosts show strong cosmic evolution in comoving number density, the fraction of such galaxies hosting active nuclei and the comoving X-ray energy density. The integrated X-ray luminosity function is used to estimate the amount of the accreted black hole mass in these AGNs and places a strong lower limit of 12% to the fraction of local low-mass galaxies hosting black holes, although a more likely value is probably much higher (>50%) once the heavily obscured objects missed in current X-ray surveys are accounted for.

Subject headings: galaxies: nuclei – galaxies: active – X-rays: galaxies

1. INTRODUCTION

Active galactic nuclei (AGNs), the manifestation of accretion onto massive black holes (MBHs), have been recognized as a critical ingredient in galaxy formation and evolution. The demography of local galaxies suggests that most – perhaps all – massive galaxies host MBHs at their centers and that MBH masses are correlated with the galaxy bulge properties (Kormendy & Richstone 1995; Magorrian et al. 1998; Gebhardt et al. 2000; Ferrarese & Merritt 2000; Häring & Rix 2004), implying the coevolution of the galaxy and MBH. The good match between the local BH mass density and the mass density of AGN relics further suggests that all massive galaxies have experienced an AGN phase during their evolution (e.g. Aller & Richstone 2002; Shankar et al. 2004; Marconi et al. 2004). Energy feedback from AGNs to their host galaxies is invoked to explain different aspects of massive galaxy evolution. AGNs may serve as the heating sources for cooling flows in clusters (e.g. McNamara & Nulsen 2007). They may suppress star formation in their host galaxies and cause them to migrate from the blue cloud to the red-sequence in the color-magnitude plot (Croton et al. 2006; Nandra et al. 2007; Georgakakis et al. 2008) and they may account for "down-sizing" galaxy evolution (e.g. Cowie et al. 1996). As the most abundant population in the universe, low-mass (defined as stellar mass $M_* < 2\times10^{10}$ $M_\odot$ through this paper) galaxies act as the building blocks of massive galaxies. However, the current understanding of MBHs' role in low-mass galaxy evolution is limited, leaving us with some basic questions: Is the existence of BHs in low-mass galaxies as common as it is in massive galaxies? Are there two types of low-mass galaxy populations (i.e. ones with BHs vs. ones without BHs)? How many low-mass galaxies experience an AGN phase? All of these questions are related to a more basic astrophysical problem: what is the black hole occupation function (BHOF; the fraction of galaxies hosting either active or quiet BHs) in low-mass galaxies?

Searching for BHs in low-mass systems offers an unique opportunity to extend the MBH-σ correlation for massive galaxies, which not only tests the universality of the relation but also is required to understand the origin of the relation. Although the MBH-σ relationship has been confirmed for low-mass systems in the local universe (Barth et al. 2005), some works suggest that the MBH-σ relationship may be replaced at low mass by a similar relation involving compact stellar nuclei (Wehner & Harris 2006; Ferrarese et al. 2006; Rossa et al. 2006).

A better understanding of primordial MBH seed growth in the early universe may also benefit from the study of BHs in low-mass galaxies, as such work could reveal aspects of the accretion mode in a low gravitational potential and low metallicity environment and of the relative importance of mass growth through accretion and merging processes. For example, in low-mass galaxies, the impulsive kick from anisotropic gravitational emission during BH-BH mergers is thought to be strong enough to eject central BHs (Favata et al. 2004; Merritt et al. 2004). Understanding AGN activity in low-mass galaxies can further constrain MBH seed formation theories. In a cold dark matter universe, the primordial MBH seeds form as remnants of Population III stars (e.g. Madau & Rees 2001) or through the direct collapse of pre-galactic gas disks (Lodato & Natarajan 2006). The efficiencies in different formation scenarios predict a wide range in the local BHOF in low-mass galaxies which can vary from zero to unity, while the prediction of the BHOF in massive galaxies is invariably unity as constrained by observations (Volonteri et al. 2008).

The current study of BHs in low mass galaxies is mostly limited to low redshift ($z < 0.3$). Despite a variety of investigations, it is still unclear how many local low-mass galaxies harbor BHs. The dynamical searches for MBHs have confirmed the existence of a BH in M32 (Verolme et al. 2002), but

---

[1] Steward Observatory, University of Arizona, 933 N Cherry Ave, Tucson, AZ 85721, USA
[4] UCO/Lick Observatory, Department of Astronomy and Astrophysics, University of California, Santa Cruz, CA 95064
[7] Spitzer Fellow

not in M33 (Merritt et al. 2001; Gebhardt et al. 2001) or NGC205 (Valluri et al. 2005). Searching for actively accreting BHs (i.e. AGNs) has provided a stronger lowerlimit and more complete view of local BHOFs as a function of the system mass through optical emission lines (e.g. Filippenko & Sargent 1989; Maiolino & Rieke 1995; Ho et al. 1995; Kauffmann et al. 2003a; Greene & Ho 2004, 2007c; Decarli et al. 2007; Dong et al. 2007; Shields et al. 2008), mid-infrared line selections (Satyapal et al. 2007, 2008) and X-ray emission (e.g. Gallo et al. 2007; Ghosh et al. 2008). It has been shown that the fraction of galaxies hosting active BHs depends on both BH mass and galaxy stellar mass, peaking at an intermediate mass range and falling toward higher and lower mass (Kauffmann et al. 2003a; Heckman et al. 2004; Greene & Ho 2007b).

As the local BH masses are most likely accumulated at high redshift, the search for AGN activity in low-mass galaxies at high redshift should provide independent and possibly better constraints on the local BHOF. Such study is also significant for understanding the evolution of nuclear activity in low-mass galaxies and the role of AGNs in low-mass galaxy evolution. With the advent of deep *Chandra* and *XMM-Newton* X-ray surveys, we have searched for X-ray emitting AGNs in low-mass host galaxies out to $z \sim 1$. In this paper, we first describe the identification of AGNs in low-mass galaxies (see § 2 and § 3). We then present the $1/V_{\rm max}$ method to correct for incompleteness in § 4 and study their spatial number density and X-ray luminosity function in § 5. In § 6, we discuss the local BHOF in low-mass galaxies constrained by our study of high redshift AGNs in such galaxies. Our conclusions are presented in § 7. Throughout this paper, "low-mass" refers to normal galaxies or AGN host galaxies with stellar mass $M_{*} < 2{\times}10^{10}$ M$_{\odot}$ and "massive" indicates those with stellar mass $M_{*} > 2{\times}10^{10}$ M$_{\odot}$. We adopt a cosmology with H_0=70 km s^{-1} Mpc^{-1}, $\Omega_{\rm m}$=0.3 and Ω_{Λ}=0.7. All magnitudes are defined in the AB system.

2. DATA: X-RAY SURVEY FIELDS

We have searched for AGNs in low-mass host galaxies in five *Chandra* and *XMM-Newton* fields, including the All-Wavelength Extended Groth Strip International Survey (AEGIS), the *Chandra* Deep Field-North Survey (CDF-N), the *Chandra* Deep Field-South Survey (CDF-S), the *Chandra* Large-Area Synoptic X-Ray Survey (CLASXS) and the *XMM-Newton* Large Scale Structure Survey (XMMLSS). Table 1 lists the properties of these five fields, including the area, the limiting hard X-ray flux, the available optical/near-IR photometry, the definition of secure (multiple-line) spectroscopic redshifts and the associated references.

All the X-ray fields are fully covered by optical/near-IR photometry. For the CDF-N, CDF-S and CLASXS fields, spectroscopic observations have been obtained for X-ray sources, while the redshifts of X-ray objects in the remaining two fields are obtained by matching X-ray catalogs to galaxy redshift survey catalogs. Table 2 summarizes the total number of X-ray sources and of spectroscopic targets. The search radii for optical counterparts to the X-ray sources are 2.0″ and 2.5″ for the *Chandra* and *XMM-Newton* fields, respectively. The optical counterparts are identified using *R*-band catalogs, which generally provide the deepest observations. If multiple optical objects within a search aperture are present, the closest one is defined as the optical counterpart. The fraction of X-ray objects with multiple optical sources within a single aperture is only $\sim$ 10%. Therefore, the assumption of adopting the closest one as the optical counterpart should not affect our conclusions. We have limited our study to objects with secure spectroscopic redshifts (see § 3) and thus the majority of the optical counterparts are brighter than 24 in the *R*-band. At R <24, the surface density of galaxies and stars is about 16.6 arcmin^{-2} (Capak et al. 2004). The probability for chance superposition between X-ray and optical sources is 6% and 10% for the *Chandra* and *XMM-Newton* fields, respectively. Given a total of 32 low-mass AGN hosts in the *Chandra* fields and zero in the *XMM-Newton* field, we have estimated that only two objects are expected to have spurious optical counterparts. Our sample only includes the X-ray sources with detected hard X-ray fluxes, defined in the energy range of 2-8 keV. The published 2-10 keV fluxes in the AEGIS and XMMLSS fields have been corrected to 2-8 keV on the assumption of a power-law photon index of 1.0, which is the average of hard-X-ray selected objects based on the hardness ratio (Nandra et al. 2005).

All optical type 1 AGNs are excluded as their nuclear radiation contaminates the host optical/near-IR light severely. Due to lack of access to the observed spectra, the definition of optical type 1 AGNs is not completely universal over all the fields. In the CLASXS field, type 1 objects are defined by having an emission line FWHM > 1000 km s^{-1}, while FWHM > 2000 km s^{-1} is adopted for the CDF-N and CDF-S fields. For the AEGIS and XMMLSS field, we have downloaded the spectra and classified type 1 objects using FWHM > 1000 km s^{-1}. In the AEGIS field, some fraction of type 1 objects is still included in the sample as the DEEP2 spectral coverage misses the permitted lines (Hα, Hβ and MgII2800$\AA$) in certain redshift windows ($\sim$0.2-0.3 and $\sim$0.6-1.2). Given a broad line AGN fraction of 16% within broad-line-detectable redshift ranges (0-0.2 and 0.3-0.6) and a total of eight AGNs in low-mass hosts within broad-line-undetectable redshift ranges in the AEGIS field, only one object in our final sample may be misclassified as an optical type 2 AGN.

3. SELECTION OF AGNS IN LOW-MASS HOST GALAXIES

Objects are identified as active low-mass galaxies if they satisfy the following two criteria: 1.) stellar mass $M_{*} < 2{\times}10^{10}$ M$_{\odot}$, our definition of *low-mass* galaxies and 2.) hard X-ray luminosity $L_{2-8{\rm keV}} > 10^{42}$ erg s^{-1}, indicating an *active* nucleus.

We have measured stellar masses by comparing the observed SEDs (i.e., the photometric data included in Table 1) to 102168 stellar synthesis models produced by Bruzual & Charlot (2003)'s code. As listed in Table 3, the stellar models span a wide range of parameter space, including metallicity, extinction, characteristic timescale of exponential star formation history, fraction of ejected gas being recycled and galaxy age. To account for the possible existence of low metallicity and young galaxies, we have included all six available metallicities and galaxy ages starting at 10^6 yrs. The fit algorithm is similar to that of Bundy et al. (2006) who have used a Bayesian

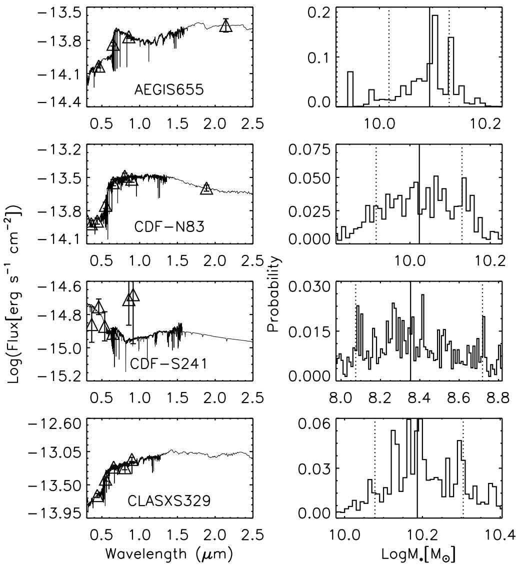

FIG. 1.— Examples of the best-fit SEDs and the probability distribution of the stellar mass of AGNs in low-mass galaxies in each field, where the solid line is the median stellar mass and two dotted lines indicate the 16 % and 84 % probability tails, respectively.

technique as described in Kauffmann et al. (2003c). In summary, for an individual object, the best-fit stellar mass is obtained for each model that corresponds to an age younger than the cosmic age at the redshift of the object. The associated χ^2 gives the probability (exp(-χ^2/2)) that this model represents the observed SED. The final probability distribution of the stellar mass is obtained by summing all probabilities within a certain mass bin. We adopted a bin width of 0.01 in logM_*, which on average contains 300 models. The median value of the stellar mass probability distribution is adopted as the final mass of a galaxy. Compared to the minimum χ^2 derived stellar mass, the mass obtained by this technique suffers much less from model degeneracies. The 68% uncertainty range of the derived stellar mass is defined by excluding the 16% tail at each end of the probability distribution. Note that this uncertainty mainly reflects the photometric errors. For the objects in the CDF-N and CLASXS fields, there are no published photometric errors. We have adopted universally an uncertainty of 0.07 magnitude, which is roughly the sky noise for a m_R=24 object in these two fields. A small fraction of objects in AEGIS, CDF-S and XMMLSS with very small photometric errors show large minimum reduced χ^2, indicating our stellar models are not able to produce the observed SEDs accurately. To estimate the uncertainty for these objects, we increased their photometric errors to 0.02 magnitude, which gives a reasonable minimum χ^2 (< 10) and larger uncertainty.

We do not include other systematic errors for our measured stellar masses, such as the accuracy of the Bruzual & Charlot (2003) code itself and possible alternative choices for the initial mass function. Our sample only includes narrow-line AGNs and thus AGN light contamination to the host emission should be small. For obscured AGNs, the scattered nuclear light may be strong (Zakamska et al. 2006). However, such scattered emission may affect the host light importantly only in the UV band. To avoid the dust emission from AGN dusty tori, we have not used photometry in the mid-IR. Fig. 1 shows examples of the observed SED superposed with the minimum-χ^2 stellar model and the probability distribution of the stellar mass for each field.

A mass cut of $< 2\times10^{10}$ M$_\odot$ is adopted to define the sample of low-mass host galaxies. Selecting the sample at this mass threshold is of interest because the properties of galaxies and BHs may transition around this mass. Studies of low-redshift galaxies have shown that galaxy properties (star formation history, size and internal structure) show significant differences at the dividing stellar mass of 3×10^{10} M$_\odot$ (Kauffmann et al. 2003b). In addition, galaxies with stellar mass $< \sim10^{10}$ M$_\odot$ often harbor compact stellar nuclei at their centers, which follow the MBH mass-bulge relationships, but which are rare in more massive galaxies (Carollo et al. 1998; Laine et al. 2003; Wehner & Harris 2006; Ferrarese et al. 2006). These stellar nuclei may be replacements for MBHs in low-mass systems where the gravitational potential is not sufficiently deep to form a BH. Furthermore, the fraction of galaxies hosting active BHs depends on the galaxy stellar mass (Kauffmann et al. 2003a; Heckman et al. 2004; Greene & Ho 2007b). In the most complete local AGN sample, the AGN fraction in galaxies fainter than M_B = -20 ($\sim10^{10}$M$_\odot$) is on average half of the fraction in brighter ones (Ho et al. 1997).

The $L_{2-8\mathrm{keV}} > 10^{42}$ erg s^{-1} AGN selection criterion is mainly based on the energy budget argument that star-forming galaxies rarely produce such high hard X-ray luminosities (e.g. Zezas et al. 1998). The resulting sample of AGNs in low-mass hosts contains 32 objects as listed in Table 4. Each object is labeled by the field name followed by the sequence number in the X-ray catalog of each field (see Table 1 for references). Fig. 2 shows distributions of low-mass AGN properties, including redshift, host stellar mass, 2-8 keV rest-frame luminosity and X-ray to R-band flux ratio.

Best et al. (2005) have measured average ratios of BH masses to the galaxy stellar mass as a function of stellar masses for the SDSS galaxy and AGN samples (see their Fig.1), where the BH mass is measured through the stellar veloclity dispersion and the MBH-σ relation. By assuming that our X-ray selected AGN sample has the same BH-to-galaxy mass ratio as the SDSS AGN, we can estimate the Eddington ratio for galaxies with M_*= 2×10^{10} M$_\odot$ and $L_{2-8\mathrm{keV}}$=10^{42} erg s^{-1}. By assuming the $L_{\mathrm{bol}}/L_{2-10\mathrm{keV}}$ = $17(L_{2-10\mathrm{keV}}/10^{43}$ erg s$^{-1})^{0.43}$ (Shankar et al. 2004) and $L_{2-8\mathrm{keV}}/L_{2-10\mathrm{keV}}$=0.86 (assuming a power law photon index of 1.0), we have an Eddington ratio of 0.007. As shown in § 4, although we can detect galaxies with stellar masses down to around 10^8 $M_\odot$, our sample is complete down to stellar mass of $10^{9.7}$ M$_\odot$ out to redshift of 0.7. For this stellar mass, the black hole mass is on average 3×10^6 M$_\odot$ (Best et al. 2005) and the corresponding Eddington ratio is 0.02 for $L_{2-8\mathrm{keV}}$=10^{42} erg s^{-1}. As a comparison to those local low-mass AGNs, our sample may be not deep enough to include the local classical low-mass Seyfert galaxies similar to NGC 4395 or POX 52, but should include galaxies similar to some low-mass SDSS AGNs found by Greene & Ho (2004, 2007c).

To better understand the role of AGNs in low-mass galaxy evolution, we will compare the sample of low-mass

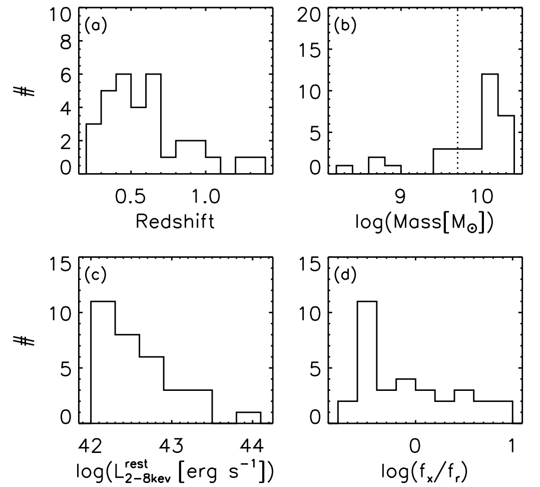

FIG. 2.— Distributions of properties of AGNs in low-mass galaxies: (a)– redshift distribution; (b) – distribution of host stellar masses where the dotted line indicates the completeness cut of $10^{9.7}$ M$_\odot$; (c) – distributions of the rest-frame 2-8 keV X-ray luminosity; (d) – distribution of X-ray to R-band flux ratio. To be complete, our number density and X-ray luminosity function for AGNs in low-mass hosts are measured for those at $0.1 < z < 0.7$, $10^{9.7}$ M$_\odot$ $< M_* < 10^{10.3}$ M$_\odot$ and $L^{\rm rest}_{\rm 2-8kev} > 10^{42}$ erg s^{-1}.

host AGNs to a sample of AGNs in massive host galaxies. The comparison sample is defined as stellar mass $M_* > 2\times10^{10}$ M$_\odot$ and $L_{\rm 2-8keV} > 10^{42}$ erg s^{-1}.

4. INCOMPLETENESS CORRECTIONS AND WEIGHTS

4.1. *The 1/V*$_{\rm max}$ *method*

The spatial number density of AGNs as a function of AGN host mass and the X-ray luminosity function of AGNs in low-mass hosts was calculated using the $1/V_{\rm max}$ method (Schmidt 1968). This calculation used those objects with $R < 24$, $L^{\rm rest}_{\rm 2-8keV} > 10^{42}$ erg s^{-1} and $M_* > 5\times10^9$ M$_\odot$ and in two redshift intervals of $0.1 < z < 0.4$ and $0.4 < z < 0.7$. $L^{\rm rest}_{\rm 2-8keV}$ is the rest-frame 2-8 keV flux assuming a photon index of 1.0 but not correcting for extinction. The maximum volume over which an object is included in the sample is given by

$$V_{\rm max} = \int_{z_{\rm low}}^{z_{\rm high}} \Omega \frac{dV}{dz} dz, \qquad (1)$$

where $[z_{\rm low}, z_{\rm high}]$ is the redshift range of interest and Ω is the solid angle covered by the X-ray survey at the flux level of the object. While $z_{\rm low}$ is always fixed to the low end of a redshift interval, the maximum redshift, $z_{\rm high}$ is defined as:

$$z_{\rm high} = \min(z^{\rm high}_{\rm bin}, z^{\rm limit}_{\rm xray}, z^{\rm limit}_{R}), \qquad (2)$$

where $z^{\rm high}_{\rm bin}$ is the high end of a redshift interval, $z^{\rm limit}_{\rm xray}$ is the limiting redshift at which the observed X-ray flux reaches the limiting flux in a given field where the K-correction is determined by assuming a power law spectrum with photon index of 1.0 and $z^{\rm limit}_{R}$ is the limiting redshift where the observed R-band magnitude reaches $m^{\rm limit}_{\rm R}$=24. To determine the K-correction in the R-band, we have redshifted the minimum reduced χ^2 spectrum model produced in our stellar mass calculations to measure the R-band magnitude at different distances.

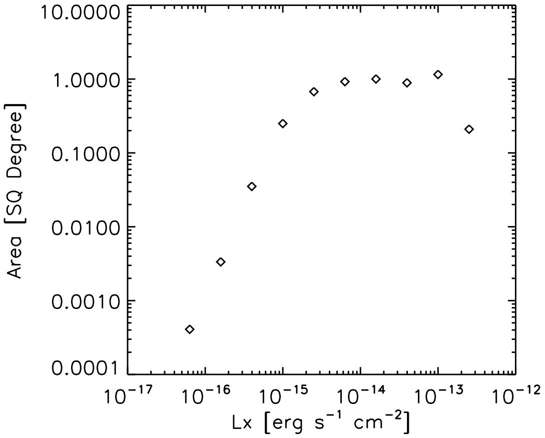

FIG. 3.— The effective solid angle as a function of the hard X-ray flux for objects in AEGIS, CDF-N, CDF-S and CLASXS fields.

As the sensitivity of the X-ray telescope shows energy and positional dependence (for details, see Yang et al. 2004), to obtain a simple estimate of the solid angle at a given hard X-ray flux, we have followed Barger et al. (2005) by comparing the observed number of X-ray objects at different hard X-ray fluxes with the average X-ray number counts from Cowie et al. (2002) and Yang et al. (2004). The sample for comparing number counts is composed of all spectroscopically observed (not only those with secure redshifts) X-ray objects in the field of CDF-N, CDF-S and CLASXS and all X-ray sources in the AEGIS field. Table 2 lists the number of X-ray objects and the number of spectroscopic targets in all the fields. The spectroscopic targets are randomly selected for the CDF-S and CLASXS fields. Although the target selection in the CDF-N field has a little bias, the majority of sources (439 out of 503) have been included in the spectroscopic sample, making the effect of this bias on the solid angle measurement negligible (Barger et al. 2005). Note that we have used the Alexander et al. (2003) X-ray catalog in the CDF-S due to its high X-ray positional accuracy so that our catalog contains ∼30 less objects than in Barger et al. (2005). The AEGIS field contains 1318 objects and the redshift is obtained by matching the X-ray catalog to the DEEP2/AEGIS catalog whose target selection depends on apparent magnitude and color. Therefore, for the objects in the AEGIS field, we have applied weights as shown below. Fig. 3 shows the effective solid angle as a function of the hard X-ray flux. At the flux of 10^{-14} erg s^{-1} cm^{-2}, it is dominated by the CLASXS (0.4 square degree) and AEGIS fields (0.67 square degree).

We have followed the method in Willmer et al. (2006) to determine the galaxy weights, ω, for the X-ray objects in the AEGIS field. These weights are used to account for the under-sampling of the photometric catalog (i.e. the fraction of objects with spectroscopic observations) and the redshift success rate of the spectroscopic catalog (i.e. the fraction of spectroscopic targets with secure redshift) of the DEEP2 observations. Briefly, we define a X-ray-optical photometric catalog as all AEGIS X-ray objects that have optical counterparts in Coil et al. (2004). Here we assume that AEGIS X-ray objects without optical counterparts (about 25% of the whole X-ray sample) are not of interest for our study of low-mass systems at $z <$

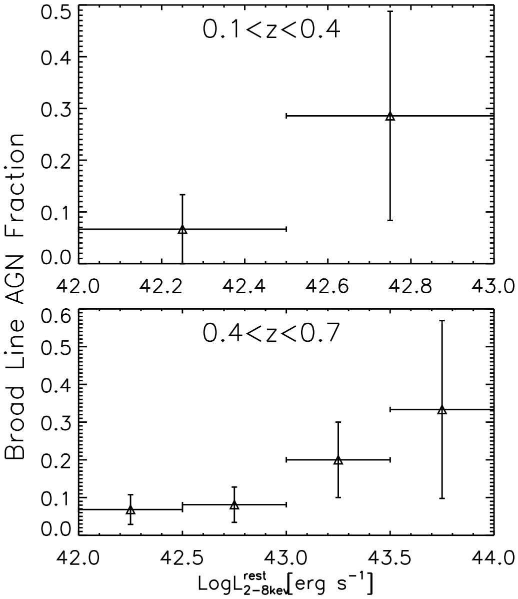

FIG. 4.— The broad line AGN fraction in two redshift intervals of $0 < z < 0.4$ and $0.4 < z < 0.7$.

0.7, either at higher redshift or with stellar mass lower than our completeness limit ($10^{9.7}$ M$_\odot$). To demonstrate this, we found that 15% of the X-ray objects without optical counterparts have $L_x > 10^{42}$ erg s^{-1} at z=0.7, i.e. satisfy the AGN definition. However, none of these objects have absolute R-band magnitude for $m_R = 24.75$ at z=0.7 brighter than any of the observed low-mass AGN hosts with $9.7 < \mathrm{Log}(M_*/M_\odot) < 10.3$, where $m_R = 24.75$ is the completeness cut of the DEEP2 photometry catalog (Coil et al. 2004). For each AEGIS X-ray object with a secure spectroscopic redshift and probability of being a galaxy $P_{\rm gal} > 0.2$, a data cube in the magnitude-color-color (R-(B-R)-(R-I)) space is defined. Then a probability for being within the permitted redshift limit [0.1, 1.4] is calculated for each object in the X-ray optical photometric catalog within this data cube. The sum of all these probabilities within the data cube divided by the number of successful redshifts gives the weight ω, which is further corrected for the probability of being placed in the slit mask.

As discussed in § 2, type 1 AGNs are excluded from the sample and thus a weight is applied to correct for their omission. The fraction of type 1 AGNs as a function of the X-ray luminosity is constructed in both redshift intervals as shown in Fig. 4, which is almost the same as the result obtained by Barger et al. (2005). The weight is calculated for each object based on the X-ray luminosity. As shown in Fig. 4, the corrections are small, as our AGN sample does not extend toward high X-ray luminosity where the broad line fraction is large. Therefore, our results throughout the paper do not change significantly if the broad-line AGN fraction does not apply.

Finally, the mass function and X-ray luminosity function are determined as:

$$\Phi(X)dX = \sum \omega/V_{\rm max}dX, \tag{3}$$

where X is the stellar mass or X-ray luminosity, respectively, ω is the galaxy weight, and $V_{\rm max}$ is the maximum volume for its detection.

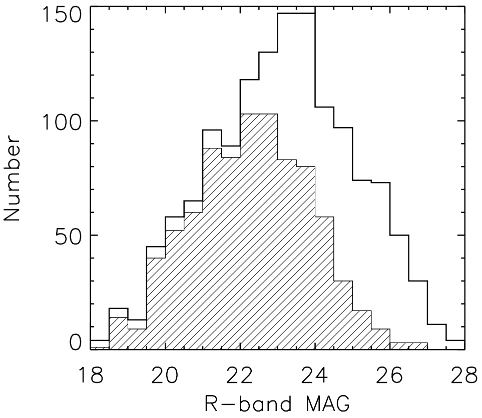

FIG. 5.— The number distribution of all spectroscopic targets (open) and objects with secure spectroscopic redshift (hatched).

4.2. *Incompleteness*

Our AGN sample where the $1/V_{\rm max}$ method applies are objects with secure spectroscopic redshifts, R <24, M_* $> 5 \times 10^9$ M$_\odot$, and $L^{\rm rest}_{\rm 2-8keV} > 10^{42}$ erg s^{-1}. The criteria of secure spectroscopic redshifts does not introduce any significant incompleteness. Fig. 5 shows the distribution of R-band magnitude for the spectroscopically observed X-ray objects (open histogram) and the objects with secure spectroscopic redshifts (filled histogram). The redshift success rate is 76% and 68% for spectroscopically observed objects at R <24 and $22 < R$ <24, respectively. Most of the spectroscopically failed objects have $22 < R$ <24. Barger et al. (2005) have shown that most objects with failed spectroscopic redshifts have photometric redshifts larger than ∼1. A similar result is found in DEEP2 (Willmer et al. 2006). A rough estimate shows that all the spectroscopically failed objects contain roughly only two low-mass AGN hosts at $z < 0.7$, given that ∼25% of the spectroscopically failed objects with $22 < R$ <24 have a photometric redshift smaller than 0.7 and that 5% of the objects with secure redshift with $22 < R$ <24 are of low mass.

The limiting R-band magnitude of 24 is deep enough to sample most low-mass galaxies with $M_* > 5 \times 10^9$ M$_\odot$ out to a redshift of 0.7, the upperlimit where the spatial number density is measured. This is because 80% of AGNs with host $M_* > 5 \times 10^9$ are detectable beyond a redshift of 0.7. The omission of a small fraction of low-mass hosts should not affect the comoving number density as they have been accounted for in the $1/V_{\rm max}$ method. To further demonstrate that the $R < 24$ limit does not introduce any significant incompleteness even in the high redshift interval ($0.4 < z < 0.7$), we carried out a Monte-Carlo simulation to demonstrate that if the comoving number density is constant within $0.4 < z <$ 0.7, the $1/V_{\rm max}$ method can re-produce the intrinsic spatial density, regardless of the loss of a small fraction of faint R-band sources. Briefly, we randomly populated the volume with AGNs to a total number similar to that observed for $0.4 < z < 0.7$. Their SEDs are assigned randomly to be one of those at $0.1 < z < 0.4$ where the limiting R-band magnitude of 24 should detect all low-mass galaxies with $M_* > 5{\times}10^9$ M$_\odot$. This is because

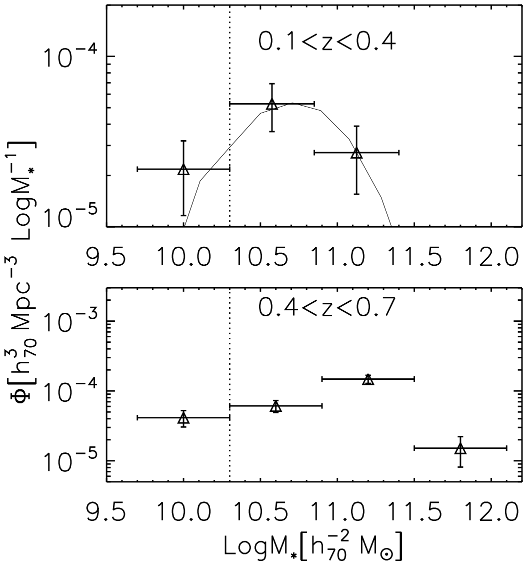

FIG. 6.— The stellar mass function of AGN hosts with $L^{\rm rest}_{2-8keV}$ $> 10^{42}$ erg s^{-1} in the two redshift intervals of $0.1 < z < 0.4$ and $0.4 < z < 0.7$. Dotted lines show the dividing mass between low-mass and massive hosts. The solid line in the upper panel shows the SDSS AGN result at $z < 0.3$ obtained by multiplying the fraction of galaxies hosting AGNs from Kauffmann et al. (2003a) with the galaxy mass function at $0.2 < z < 0.4$ from Pérez-González et al. (2008). The normalization of the AGN fraction of Kauffmann et al. (2003a) has been decreased by a factor of 8 to match our normalization (a discussion about the difference between the SDSS and our low-redshift samples can be found in § 5.3).

the Bruzual & Charlot (2003) oldest simple stellar populations with solar metallicity and $M_* = 5\times10^9$ M$_\odot$ have m_R=24 at z=0.4. Younger or lower metallicity galaxies will emit higher luminosities. We then applied the measured $z_R^{\rm limit}$ to the simulated galaxies and measured the $1/V_{\rm max}$-based spatial number density. A thousand simulations show that there is no systematic difference in our estimate of the spatial density. For the incompleteness due to the X-ray detection threshold, since all AGNs (defined as $L^{\rm rest}_{\rm 2-8keV} > 10^{42}$ erg s^{-1}) in low-mass hosts with $M_* > 5\times10^9$ have $z^{\rm limit}_{\rm Xray} > 0.7$, the $1/V_{\rm max}$ method should recover the real spatial number density.

5. RESULTS

5.1. *Comoving Number Density and AGN Fraction*

Fig. 6 shows the spatial number density of AGNs with $L^{\rm rest}_{\rm 2-8keV} > 10^{42}$ erg s^{-1} as a function of AGN host mass in the two redshift intervals of $0.1 < z < 0.4$ and $0.4 < z < 0.7$. Dotted lines show the dividing mass between low-mass and massive hosts. In both redshift intervals, the AGN number density depends on the host mass, peaking at an intermediate mass range and decreasing toward higher and lower mass. Furthermore, the AGN host mass function peaks at a higher mass in the higher redshift interval. Our low redshift interval suffers from low number statistics with on average ∼7 objects per mass bin, compared to ∼20 objects per mass bin in high redshift interval. However, the peak around a stellar mass of $10^{10.3}$ - $10^{10.8}$ M$_\odot$ is quite possibly real. For example, Greene & Ho (2007b) have measured the local BH mass function of type 1 SDSS AGNs at $z < 0.3$. Although suffering from an incompleteness problem, there appears to be a turnover of their BH mass function around a BH mass of 10^7 M$_\odot$, which corresponds on average to a host stellar mass of $10^{10.2}$ M$_\odot$ (Best et al. 2005). The statistical significance for the low-redshift AGN host mass function peaking in the second mass bin was estimated using a Monte-Carlo simulation. Basically, we perturbed the mass function at each mass bin ten thousand times assuming a normal distribution with the 1-σ deviation equal to the measured error. The probabilities for the peak at first, second and third bins are 10%, 80% and 10%, respectively, which indicates that the low-redshift AGN host mass function most likely peaks in the second mass bin.

To further demonstrate that the AGN host mass function peaks at a higher mass in our high redshift interval, the solid line in the upper panel of Fig. 6 shows the SDSS AGN result at $z < 0.3$ obtained by multiplying the fraction of galaxies hosting AGNs from Kauffmann et al. (2003a) with the galaxy mass function at $0.2 < z < 0.4$ from Pérez-González et al. (2008). The galaxy mass function obtained by Pérez-González et al. (2008) is based on a rest-frame near-IR selected galaxy sample and is generally consistent with results of other studies (any differences are within 0.3 dex (see their Fig.4)). At $z < 0.7$, the result of Pérez-González et al. (2008) is complete down to stellar mass of 10^9 M$_\odot$, deep enough for our purpose. The normalization of the AGN fraction of Kauffmann et al. (2003a) has been decreased by a factor of 8 to match our normalization (a discussion about the difference between the SDSS and our low-redshift samples can be found in § 5.3). With much higher number statistics, the SDSS result shows the AGN host mass function peaks around $10^{10.7}$ M$_\odot$. We then carried out a simulation by assuming the $0.4 < z < 0.7$ AGN mass function actually follows the SDSS result at $z < 0.3$. For each object at $0.4 < z < 0.7$, a host mass is assigned randomly with a relative probability that follows the SDSS result. The range of simulated stellar mass is from 10^9 to $10^{12.5}$ M$_\odot$. We also assumed that the total probability in this mass range is equal to 1. Combining the simulated stellar mass and the observed $z^{\rm limit}_{\rm xray}$ and $z_R^{\rm limit}$ measured in § 4, we can construct the AGN mass function at $0.4 < z < 0.7$ using the same mass bins as for the observed data. Ten thousand simulations indicate that the probability is 99.6% for the mass function to peak in one of the two lowest mass bins. That is, the simulated host mass function at $0.4 < z < 0.7$ (using the SDSS low-z data as the basis of the simulated data) would likely (99.6%) peak in the two low-mass bins (i.e. $< 10^{11}$ M$_\odot$), while the observations at $0.4 < z < 0.7$ find a significant peak at higher mass ($> 10^{11}$ M$_\odot$). This result indicates that the tendency for the AGN mass function in the high redshift interval to peak at higher mass is significant (99.6%).

The simulations shown above test the pure number statistics. In order to account for the possible selection bias that the low-mass galaxies harbor faint AGNs due to the mild correlation between the galaxy stellar mass and the central BH mass coupled with a given Eddington ratio distribution, we first created a set of stellar masses with the relative probability following the galaxy stellar mass function from Pérez-González et al. (2008). These stellar masses were then converted to the BH mass distribution using the average ratios of BH masses to galaxy

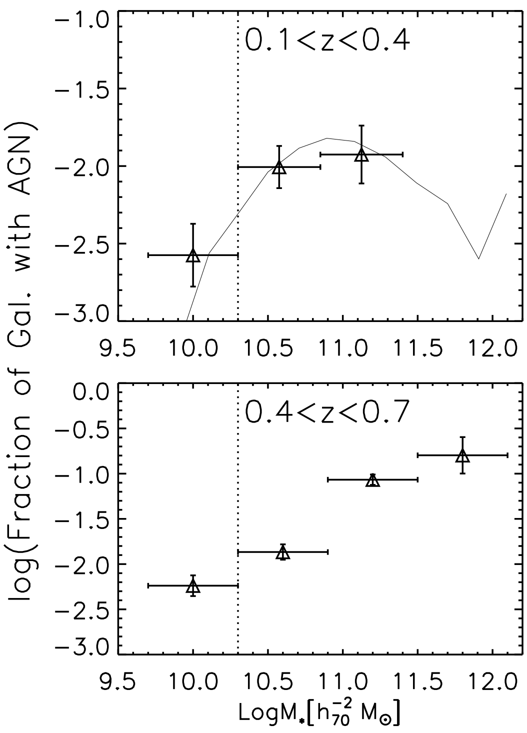

FIG. 7.— The fraction of galaxies hosting active nuclei as a function of host stellar mass in the two redshift intervals of $0.1 < z < 0.4$ and $0.4 < z < 0.7$. Dotted lines show the dividing mass between low-mass and massive hosts. The solid line in the upper panel shows the trend of the SDSS powerful AGN fraction with the host stellar mass from Kauffmann et al. (2003a) whose normalization has been decreased by a factor of 8 (a discussion about the difference between the SDSS and our low-redshift samples can be found in § 5.3).

stellar masses as a function of stellar masses and associated errors from Best et al. (2005). For the Eddington ratio between [10^{-5}, 1], we assumed a probability distribution of $P(L_{\rm bol}/L_{\rm Edd})\ {\rm d}(L_{\rm bol}/L_{\rm Edd}) \propto 1/(L_{\rm bol}/L_{\rm Edd})^n$, where n is a free parameter. By assuming $L_{\rm bol}/L_{\rm x} = 20$, the simulated AGN sample is then defined as objects with $L_{\rm x} > 10^{42}$ erg s^{-1} and the host mass function of this sample can be constructed. We simulated about ten times for each n value which is given in a set of discrete numbers starting at zero and increasing in a step of 0.5. At n=2, the simulated AGN mass function shows a similar trend to our measured mass function in the redshift interval of $0.4 < z < 0.7$. The peak number density is about four times larger than the value around the lowest measured mass (10^{10} $M_\odot$). This result shows that when the Eddington ratio distribution is strongly biased toward a low value, the observed turnover of the AGN mass function is due to the selection bias. However, the corresponding simulated fractions of galaxies hosting AGNs are an order of magnitude lower than the observed ones. This implies the turnover of the AGN mass function most likely indicates a real decrease of the number density of galaxies with active BHs.

Compared to the galaxy mass function, the unique feature of these two AGN mass functions is that they do not increase monotonically with decreasing mass. A physical parameter more related to the AGN cycle and BHOF is the fraction of galaxies hosting active nuclei, which is defined by dividing the AGN host mass function by the galaxy mass function at a given stellar mass, as shown in Fig. 7. The $0.2 < z < 0.4$ and $0.4 < z < 0.6$ galaxy mass functions from Pérez-González et al. (2008) are used for our low and high redshift intervals, respectively. Fig. 7 shows that more massive galaxies host active nuclei more frequently in both redshift intervals. In the local universe, it has been found that the AGN fraction depends on the host stellar mass (Kauffmann et al. 2003a; Gallo et al. 2007; Decarli et al. 2007; Sivakoff et al. 2008), host Hubble type (Ho et al. 1997) and BH mass (Heckman et al. 2004; Greene & Ho 2007b). Note that these three parameters are roughly correlated with each other. In general, the fraction harboring active nuclei is lower for lower-mass local systems. Our result indicates that such a dependence also exists at high redshift. However, there are differences in the behavior between low- and high-redshift. Kauffmann et al. (2003a) show their $z < 0.3$ SDSS AGN fraction increases with stellar mass from low-mass galaxies up to galaxies with 10^{11} M$_\odot$ and then drops quickly toward higher mass galaxies, which is shown as the solid line in the upper panel of Fig. 7. Our result for $0.1 < z < 0.4$ is consistent with their work, particularly since it indicates a leveling out of the AGN fraction near 10^{11} M$_\odot$. However, our sample contains too few hosts above this limit to confirm the drop toward even higher masses. At 0.4<z<0.7, our study shows that the AGN fraction increases all the way from low-mass galaxies to massive galaxies with $M_* = 10^{12}$ $M_\odot$. Note that our AGN fraction for massive galaxies ($M_* > 10^{11}$ M$_\odot$) is consistent with other studies of X-ray AGNs at this redshift (Bundy et al. 2007; Alonso-Herrero et al. 2008), while showing that this lack of turn-over continues up to higher mass. The difference between our high redshift interval and the SDSS local universe may be explained by the cosmic "downsizing" evolution of MBHs (e.g. Barger et al. 2005). Massive BHs in massive galaxies have accumulated their masses at high redshift and become quiescent in the local universe.

Note that our AGNs are defined as those with $L^{\rm rest}_{\rm 2-8keV} > 10^{42}$ erg s^{-1}. It is obvious that the AGN number density or AGN fraction depends on the depth of surveys, or, equivalently, the limiting Eddington accretion ratio for a given BH mass. As shown in § 3, the limiting Eddington ratio is 0.02 for our lowest stellar mass of $10^{9.7}$ M$_\odot$. For a galaxy with stellar mass of 10^{11} M$_\odot$, the limiting Eddington ratio is 0.001. To have a sense of the missed fraction of AGNs with lower Eddington ratios, we used the currently most complete local AGN sample from Ho et al. (1995) as a comparison. Our sample of AGNs should miss a significant fraction of high-ionization Seyfert galaxies, as local Seyferts have a median Eddington ratio of 1.3×10^{-4} (Ho 2008). We may miss all low-ionization nuclear emission-line regions (LINERs), as none of the local LINERs has an Eddington ratio > 0.001 (Ho 2008). Overall, only 5% and 10% of all local AGNs have Eddington ratios larger than 0.01 and 0.001, respectively (Ho 2008). Therefore, the fraction of galaxies with active BHs at high redshift may be much larger than our result, which is limited to $L^{\rm rest}_{\rm 2-8keV} > 10^{42}$ erg s^{-1}. Identifying these additional AGNs is difficult because of the overlap of their X-ray luminosities

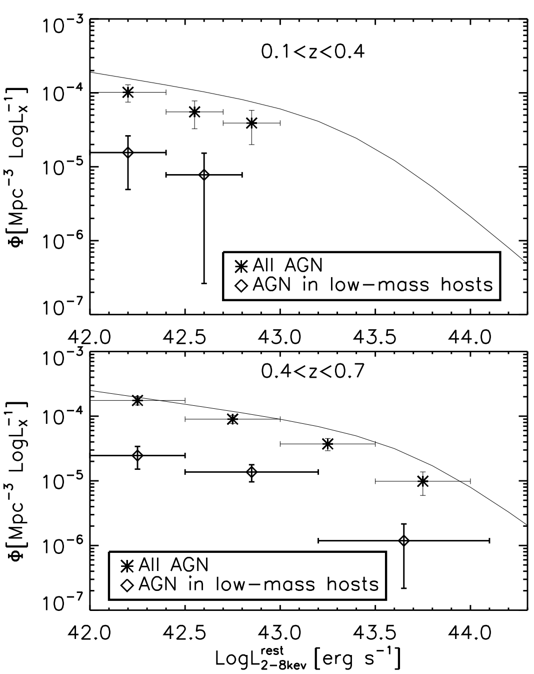

FIG. 8.— The rest-frame 2-8 KeV X-ray luminosity function of AGNs in low-mass hosts, and of all AGNs in the two redshift intervals of 0.1< z <0.4 and 0.4< z <0.7. The two solid lines show the XLF obtained by Barger et al. (2005), based on the CDFN, CDFS and CLASXS fields.

with those resulting from star formation (Ranalli et al. 2003). However, it is still important to understand the fraction of galaxies hosting AGNs with relatively high Eddington ratios and their trends with host masses, as these AGNs may be in the phase when feedback from MBHs is most important and also the main stage of BH growth through accretion.

5.2. *X-ray Luminosity Function of AGNs in Low-Mass Hosts*

Fig. 8 shows the X-ray luminosity functions of AGNs in low-mass hosts (diamonds) and all AGNs (asterisks) in the two redshift intervals of 0.1 < z <0.4 and 0.4< z <0.7. Two solid lines show the XLFs obtained by Barger et al. (2005), based on the CDFN, CDFS and CLASXS fields. The XLFs of our AGN host sample with R <24 closely match their results for the higher redshift interval. In the low redshift interval, there is about a factor of two difference in the highest luminosity bin. This is most likely caused by the cosmic variance due to the small comoving volume at low redshift.

The total X-ray energy density of AGNs in low-mass hosts can be measured by integrating the XLF where there are data points. The measurements give (2.2±1.4)×10^{37} and (1.4±0.4)×10^{38} erg s^{-1} Mpc^{-3} at $0.1 < z < 0.4$ and $0.4 < z < 0.7$, respectively. Similarly, the X-ray energy density of all AGNs can be obtained. The contribution of AGNs in low-mass hosts to the total X-ray energy density is (11±8)% and (14±5)% in the lower and higher redshift intervals, respectively. Therefore, these AGNs are energetically important to the cosmic X-ray background.

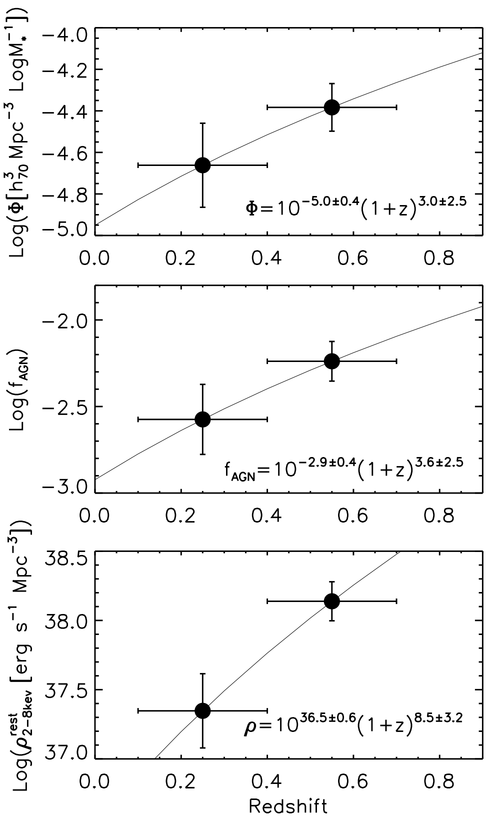

FIG. 9.— The redshift evolution of AGNs with host stellar mass $9.7 < \log M_*/M_\odot < 10.3$. From top to bottom: the comoving number density; the fraction of low-mass galaxies hosting active nuclei; and the comoving X-ray energy density.

5.3. *Redshift Evolution of AGNs in Low-Mass Hosts*

As shown in Fig. 9, AGNs in low-mass hosts show strong redshift evolution. The number density increases with redshift following $\Phi_{\rm DAGN} = 10^{-5.0\pm0.4}$ $(1+z)^{3.0\pm2.5}$ Mpc^{-3} log(M$_\odot$)$^{-1}$, the fraction of low-mass galaxies with AGNs evolves as $f_{\rm AGN} = 10^{-2.9\pm0.4}(1+z)^{3.6\pm2.5}$ and the energy density follows $\rho_{\rm DAGN} = 10^{36.5\pm0.6}(1+z)^{8.5\pm3.2}$ erg s^{-1} Mpc^{-3} in the redshift range of 0<z<0.7. Note that these three quantities are related to each other to some degree.

To evaluate our result for cosmic evolution of AGNs in low-mass galaxies, we compared it at low-redshift to those based on SDSS optical-emission-line-selected AGNs. Greene & Ho (2007b) show that the spatial number density of BHs between $10^{6.5}$ and $10^{7.5}$ M$_\odot$ hosted by SDSS narrow-line AGNs from Heckman et al. (2004) is around 6×10^{-5} Mpc^{-3} logM$_{\rm BH}^{-1}$ (see their Fig.10). Assuming the host galaxies of these BHs have $M_* \sim 10^{10}$ M$_\odot$, this number density is three times higher than the prediction of ∼(2.0±1.5)×10^{-5} Mpc^{-3} logM$_*^{-1}$ at a redshift of 0.15 based on the number density evolution of our AGNs in low-mass hosts. Note that our result has been corrected for broad-line AGN. However, the correction is quite small (∼10%) as shown in § 4.1 and Fig. 4. The difference could be partly caused by our low number statistics. Although the limiting Eddington ratios of the Greene & Ho (2007b)'s AGNs are similar to ours (∼ 0.01), the different selection algorithms (optical emission diagnostics vs. X-ray emission) may be another reason for the discrepancy. The optical emission diagnostics miss AGNs when the contrast of narrow line emission to host galaxy light is low. At low redshift, the slit for the spectroscopic observations covers only part of the host galaxies so that host galaxy light dilution is not quite so severe. Kauffmann et al. (2003a) show that the SDSS optical emission line diagnostics can recover the AGNs with Eddington ratios below 0.01 for host galaxies with $M_* \sim 10^{10}$ M$_\odot$, if the emission lines are not strongly extincted. The X-ray emission method misses AGNs whose X-ray emission is obscured so that their observed X-ray luminosity falls below our threshold for AGN definition. It is obvious that Compton-thick AGNs ($N_H > 10^{24}$ cm^{-2}) will be missed in the 2-10 keV X-ray survey. However, if AGNs in low-mass hosts have intrinsically weaker X-ray emission compared to more massive host AGNs, the heavily-extincted but Compton-thin AGNs (10^{23} cm^{-2} $< N_H <$ 10^{24} cm^{-2}) may still be missed. Our X-ray spectral fits of AGNs in low-mass hosts with X-ray counts > 100 (Shi et al. 2008, in preparation) have shown that only ∼10% of these AGNs have $N_{\rm HI} > 10^{23}$ cm^{-2}. Heckman et al. (2005) did show that the emission-line-selected AGN sample is more complete than the X-ray-selected one at low redshift and that the SDSS AGN spatial density is about three times higher than X-ray-selected AGNs. Although at low redshift optical emission line diagnostics are more complete, X-ray selection identifies more AGNs at high redshift. X-ray selection also provides more uniform selection criteria (e.g., less affected by dilution by the host galaxy extended emission). As a summary, the prediction at low-redshift based on our result of cosmic evolution of AGNs in low-mass galaxies is generally consistent with the SDSS result, with an offset caused by different selection biases between X-ray-emission-selected AGNs and optical-emission-line-selected ones.

6. DISCUSSION: BLACK HOLE OCCUPATION FRACTION IN LOW-MASS GALAXIES

6.1. *Fraction of Galaxies Hosting AGNs*

§ 5.1 shows that the AGN mass function peaks at an intermediate mass and decreases toward the low-mass regime, in contrast to the monotonic increase of the galaxy mass function. § 5.1 also indicates that the fraction of galaxies hosting active nuclei decreases with decreasing host stellar mass. Theoretically, the fraction of galaxies hosting AGNs can be estimated by

$$f_{\rm AGN} = f_{\rm BHOF}\gamma t_{\rm AGN} \qquad (4)$$

where $f_{\rm BHOF}$ is the black hole occupation function, i.e., the fraction of galaxies hosting MBHs at their centers, γ is the fractional AGN trigger rate, i.e., the fraction of MBHs becomes active per unit time, and $t_{\rm AGN}$ is the duration of a nuclear activity episode with L_X>10^{42} erg s^{-1}. The trend of AGN fractions with host mass can be caused by the host mass dependence of any one of the three factors, $f_{\rm BHOF}$, γ and $t_{\rm AGN}$. Different models for MBH seed formation in the early universe predict different mass dependences of $f_{\rm BHOF}$ (Volonteri et al. 2008). $t_{\rm AGN}$ is most likely mass dependent, as the lower mass systems require larger Eddington ratios to be brighter than L_X=10^{42} erg s^{-1}.

To get some idea of $f_{\rm BHOF}$ of low-mass galaxies, we make a simple assumption that each major merger triggers one-time nuclear activity and thus γ = the merging rate. Although the measurement of the merging rate is subject to various uncertainties (e.g. Cassata et al. 2005; Shi et al. 2006; Lotz et al. 2008), it should be around 0.1-0.2 Gyr^{-1} for massive galaxies. Simply assuming $\gamma = 0.1$ Gyr^{-1} for low-mass galaxies, we have :

$$f_{\rm BHOF} = \frac{0.03{\rm Gyr}}{t_{\rm AGN}}\frac{0.1}{\gamma}; (0.1 < z < 0.4) \qquad (5)$$

$$f_{\rm BHOF} = \frac{0.06{\rm Gyr}}{t_{\rm AGN}}\frac{0.1}{\gamma}; (0.4 < z < 0.7) \qquad (6)$$

In this simplified case, as long as the duration of one episodic nuclear active phase is not long (<0.06 Gyr), *all* low-mass galaxies with $9.8 < \log M_* < 10.3$ at $z <\sim 1$ should harbor BHs at their centers.

6.2. *Accreted BH Mass by AGNs in Low-Mass Galaxies*

The amount of BH mass accreted by AGNs in low-mass galaxies since $z = 1$ can be measured by integrating the cosmic evolution of the X-ray energy density of these AGNs obtained in § 5.3. This mass should provide a stringent lower limit to the BHOF in local low-mass galaxies. An average X-ray to bolometric luminosity correction of 19 is obtained by using $L_{\rm bol}/L_{2-10{\rm keV}} = 17(L_{2-10{\rm keV}}/10^{43}$ erg s$^{-1})^{0.43}$ (Shankar et al. 2004), $L_{2-8{\rm keV}}/L_{2-10{\rm keV}}$=0.86 and the mean X-ray luminosity of 7×10^{42} erg s^{-1}. Assuming the mass-to-radiation conversion efficiency ε=0.1, the total accreted black hole mass in galaxies with $9.7 < \log(M_*/M_\odot) < 10.3$ since $z = 1$ is $3.9(\pm0.9)\times10^3$ M$_\odot$ Mpc^{-3}.

This accreted BH mass must be hosted in local low-mass galaxies. The corresponding total galaxy mass can be estimated using the bulge-BH relation and bulge-to-disk ratio. The lower limit to the local BHOF is then the ratio of the total mass of galaxies hosting the accreted BHs to the total local mass in low-mass galaxies. In practice, we can alternatively assume all local low-mass galaxies host BHs. The lower limit of the BHOF is then the ratio of the accreted BH mass to the assumed total BH mass hosted by all local low-mass galaxies.

The BH mass function can be determined from the galaxy velocity dispersion function using the relationship between the velocity dispersion and BH mass (M_{BH}-σ). However, it is relatively difficult to measure the velocity dispersion, resulting in incompleteness of the BH mass function at the low mass end. Alternatively, it can be derived from the bulge luminosity function using the relationship between the bulge luminosity and the BH mass ($L_{\rm Bulge}$-M_{BH}). In this case, the bulge-to-disk ratios of galaxies with different morphologies are required to derive the bulge luminosity function from the galaxy total luminosity function. In practice, the two methods are actually employed at the same time to complement each other. Different studies produce a relatively consistent result for the total local BH mass density, which is around 4.5×10^5 M$_\odot$ Mpc^{-3} with uncertainty < 2.0×10^5 M$_\odot$ Mpc^{-3} (Aller & Richstone 2002; Shankar et al. 2004; Marconi et al. 2004). Therefore, the accreted BH mass by AGNs in low-mass hosts since z = 1 is only a small fraction (0.8%) of the total local BH mass density.

To estimate the BHOF in local low-mass galaxies using the accreted BH mass during their AGN phase since $z = 1$, we first need to determine the local successor of our low-mass AGN hosts. Given the cosmic evolution of the stellar mass density of galaxies with different stellar masses provided by Pérez-González et al. (2008), the $9.7 < \log(M_*/M_\odot) < 10.3$ interval at median redshift of $z = 0.5$ corresponds roughly to $9.85 < \log(M_*/M_\odot) < 10.45$ at $z = 0$. To estimate the total BH mass associated with local galaxies with $9.85 < \log(M_*/M_\odot) < 10.45$, we measured the BH mass hosted by the early-type and late-type galaxies separately, as they have different bulge to total light ratios, $f_{\rm bulge}^{\rm early} = 0.85\pm0.05$ and $f_{\rm bulge}^{\rm late} = 0.30\pm0.05$ (Shankar et al. 2004). Assuming that $\log(M_{BH}/{\rm M}_\odot) = (8.20\pm0.10)+(1.12\pm0.06)\log(M_{\rm bulge}/10^{11}{\rm M}_\odot)$ (Häring & Rix 2004), early and late type galaxies with $9.85 < \log(M_*/{\rm M}_\odot) < 10.45$ harbor BHs with $6.85 < \log(M_{BH}/M_\odot) < 7.50$ and $6.15 < \log(M_{BH}/M_\odot) < 6.80$, respectively. By fitting Fig.5 of Shankar et al. (2004) with the formula

$$\Phi = \Phi_{BH}^*(\frac{M_{BH}}{M_{BH}^*})^{\alpha+1}\exp[-(\frac{M_{BH}}{M_{BH*}})^{\beta}], \qquad (7)$$

we obtained $\Phi_{BH}^* = 5.2(\pm0.2)\times10^{-3}$ Mpc^{-3}, $M_{BH}^* = 8.8(\pm2.0)\times10^{6}$ M$_\odot$, α = -0.47($\pm$0.03) and β = 0.39($\pm$0.01) for early-type galaxies, and $\Phi_{BH}^* = 1.9(\pm0.2)\times10^{-2}$ Mpc^{-3}, $M_{BH}^* = 3.3(\pm1.7)\times10^{5}$ M$_\odot$, α = -0.57($\pm$0.09) and β = 0.34($\pm$0.02) for late-type galaxies. Integrating the above equation over the range of interest, the local early- and late-type galaxies with $9.85 < \log(M_*/M_\odot) < 10.45$ harbor total BH masses of 2.1×10^4 and 1.2×10^4 M$_\odot$ Mpc^{-3}, respectively. Therefore, the accreted BH mass by AGNs in low-mass hosts from $z = 1$ contributes 12% of the local BH mass hosted in galaxies with $9.85 < \log(M_*/M_\odot) < 10.45$.

Three main uncertainties associated with this percentage include the accreted BH mass, the stellar mass of local counterparts of our high redshift low-mass hosts and the local BH mass function. As shown above the measurement error of the accreted BH mass is about 20%. A larger uncertainty for this accreted BH mass is from the uncertain estimate of AGN accretion in low-mass galaxies at $0.7 < z < 1$. The current assumption is that it follows the trend at $z < 0.7$. If the energy density of AGNs in the low-mass host is flat at $z > 0.7$, the accreted BH mass will decrease by about a factor of 2. To estimate the second uncertainty, we can assume an extreme case where all our AGNs in low-mass hosts are at $z = 1$. In this case, the local counterparts have $10.1 < \log(M_*/M_\odot) < 10.7$ and the accreted BH mass contribution is 6%. The uncertainty in the local BH mass function is about a factor of 3, from comparing different studies (Aller & Richstone 2002; Shankar et al. 2004; Marconi et al. 2004). Therefore, the final uncertainty could be a factor of 4, estimated by adding the above errors quadratically.

A more important factor, resulting in severe underestimate of the accreted BH mass by AGNs, is the X-ray obscuration correction for the observed X-ray flux plus the significant number of missed heavily-obscured AGNs in current X-ray surveys. This problem is even worse for AGNs in low-mass hosts, as (1) they on average have low intrinsic X-ray luminosities, with many falling below our selection criteria of $L_X > 10^{42}$ erg s^{-1} and (2) the structure of the circumnuclear material may vary with the luminosity in a way that causes lower luminosity objects to be more obscured, as implied by the decrease in the fraction of type 2 objects with increasing luminosity (e.g. Barger et al. 2005). We calculated the degree of underestimation in two ways. First, we measured the accreted BH mass of 3.4×10^4 M$_\odot$ Mpc^{-3} by all X-ray-detected AGNs from $z = 1$ by integrating the X-ray energy density evolution of all AGNs (see § 5.2). Shankar et al. (2004) obtained total BH mass of $\sim1.3\times10^5$ M$_\odot$ Mpc^{-3} accreted by all AGNs from $z = 1$ with a correction for obscuration and accounting for missing Compton-thick objects. Therefore, the accreted BH mass by AGNs in low-mass galaxies is underestimated by a factor of 4, by assuming that the obscuration of these AGNs is similar to that of all AGNs. The second way is to compare the distribution of the HI column density of observed AGNs to the intrinsic distribution to estimate the fraction of missing AGNs. Our X-ray spectral fits of AGNs in low-mass galaxies with X-ray counts > 100 (Shi et al. 2008, in preparation) have shown that only 10% of such AGNs have HI column density $N_{\rm HI} > 10^{23}$ cm^{-2}. The study of local Seyfert galaxies shows that 75% of Seyfert 2 galaxies have $N_{\rm HI} > 10^{23}$ cm^{-2} (Risaliti et al. 1999). If AGNs in low-mass galaxies have structures of circumnuclear material similar to those in Seyfert galaxies, 75% of the low-mass galaxies should be missed and the accreted BH mass by all such AGNs is underestimated by a factor of 4, similar to the value estimated by the first method.

Therefore, the accreted BH mass by all AGNs in low-mass hosts including missed heavily-obscured ones from $z = 1$, probably contribute $\sim$ 50% of the local BH mass hosted in galaxies with $9.85 < \log(M_*/M_\odot) < 10.45$. As discussed at the beginning of this section, this percentage is obtained by assuming all such galaxies harbor BHs at their centers. A percentage of 50% can also be interpreted as the lower limit of the BHOF in local galaxies with $9.85 < \log(M_*/M_\odot) < 10.45$, i.e., at least 1 out of 2 local galaxies with $9.85 < \log(M_*/M_\odot) < 10.45$ harbor BHs. Accretion at higher redshift ($z > 1$), at low Eddington ratios, or the mass growth through the BH merging processes may provide the remaining BH mass.

The above results strongly favor a scenario where the nuclear activity is a necessary ingredient during low-mass galaxy evolution. The fraction of low-mass galaxies hosting active nuclei (see § 6.1) and the amount of the accreted black hole mass in low-mass host AGNs (see this section) implies that a significant fraction of low-mass galaxies in the local universe harbor black holes at their centers and these black hole masses are assembled through the active accretion phase ($L_X > 10^{42}$ erg s^{-1}) at $z < 1.0$.

7. CONCLUSIONS

We have studied a sample of X-ray AGNs in low-mass host galaxies with stellar mass of 5×10^9 M$_\odot$ $< M_* <$ 2×10^{10} M$_\odot$ out to $z \sim 1$. Our main conclusions are:

(1) By including AGNs in more massive host galaxies, we have constructed the stellar mass function of AGN host galaxies extending down to the low-mass regime in two redshift intervals of $0.1 < z < 0.4$ and $0.4 < z < 0.7$. We have found the AGN host stellar mass function peaks at an intermediate mass range, with the peak shifting toward higher mass at higher redshift.

(2) By comparing to AGNs in more massive hosts, we have found that the fraction of galaxies hosting active nuclei depends strongly on the host mass, increasing from low-mass galaxies continuously to the most massive ones. The fraction of low-mass galaxies hosting active nuclei suggests that a large fraction of such galaxies at $0 < z < 1$ harbor black holes at their centers as long as the low-mass host AGN lifetime with $L_X > 10^{42}$ erg s^{-1} is not long (< 0.06 Gyr).

(3) The X-ray luminosity functions of AGNs in low-mass hosts have been constructed in two redshift intervals of $0.1 < z < 0.4$ and $0.4 < z < 0.7$. AGNs in low-mass hosts contribute ∼10% of the X-ray energy density of all the AGNs in $0 < z < 1$, indicating that such AGNs make an energetically significant contribution to the cosmic X-ray background.

(4) AGNs in low-mass hosts show strong redshift evolution in their comoving number density, the fraction of such galaxies with active nuclei and the comoving radiation energy density. By integrating the X-ray luminosity function of these AGNs over the redshift range of $0 < z < 1$, the accreted black hole mass in galaxies with 5×10^9 $M_\odot < M_* < 2\times10^{10}$ $M_\odot$ is $(3.9\pm0.9)\times 10^3$ $M_\odot$ Mpc^{-3}. This number gives a strong lower limit of 12% to the fraction of local low-mass galaxies harboring black holes, which may be much higher (> 50%) if the dusty torus of the AGNs in low-mass galaxies has similar structure to or is more opaque than that of AGNs in massive host galaxies.

We thank the anonymous referee for detailed comments. Support for this work was provided by NASA through contract 1255094 issued by JPL/ California Institute of Technology.

REFERENCES

Alexander, D. M., et al. 2003, AJ, 126, 539

Alonso-Herrero, A., Pérez-González, P. G., Rieke, G. H., Alexander, D. M., Rigby, J. R., Papovich, C., Donley, J. L., & Rigopoulou, D. 2008, ApJ, 677, 127

Aller, M. C., & Richstone, D. 2002, AJ, 124, 3035

Barger, A. J., Cowie, L. L., Brandt, W. N., Capak, P., Garmire, G. P., Hornschemeier, A. E., Steffen, A. T., & Wehner, E. H. 2002, AJ, 124, 1839

Barger, A. J., et al. 2003, AJ, 126, 632

Barger, A. J., Cowie, L. L., Mushotzky, R. F., Yang, Y., Wang, W.-H., Steffen, A. T., & Capak, P. 2005, AJ, 129, 578

Barth, A. J., Greene, J. E., & Ho, L. C. 2005, ApJ, 619, L151

Best, P. N., Kauffmann, G., Heckman, T. M., Brinchmann, J., Charlot, S., Ivezić, Ž., & White, S. D. M. 2005, MNRAS, 362, 25

Bruzual, G., & Charlot, S. 2003, MNRAS, 344, 1000

Bundy, K., et al. 2006, ApJ, 651, 120

Bundy, K., et al. 2007, ArXiv e-prints, 710, arXiv:0710.2105

Capak, P., et al. 2004, AJ, 127, 180

Carollo, C. M., Stiavelli, M., & Mack, J. 1998, AJ, 116, 68

Cassata, P., et al. 2005, MNRAS, 357, 903

Chabrier, G. 2003, PASP, 115, 763

Chiappetti, L., et al. 2005, A&A, 439, 413

Coil, A. L., Newman, J. A., Kaiser, N., Davis, M., Ma, C.-P., Kocevski, D. D., & Koo, D. C. 2004, ApJ, 617, 765

Croton, D. J., et al. 2006, MNRAS, 365, 11

Cowie, L. L., Songaila, A., Hu, E. M., & Cohen, J. G. 1996, AJ, 112, 839

Cowie, L. L., Garmire, G. P., Bautz, M. W., Barger, A. J., Brandt, W. N., & Hornschemeier, A. E. 2002, ApJ, 566, L5

Davis, M., et al. 2003, Proc. SPIE, 4834, 161

Davis, M., et al. 2007, ApJ, 660, L1

Decarli, R., Gavazzi, G., Arosio, I., Cortese, L., Boselli, A., Bonfanti, C., & Colpi, M. 2007, MNRAS, 381, 136

Dong, X., et al. 2007, ApJ, 657, 700

Favata, M., Hughes, S. A., & Holz, D. E. 2004, ApJ, 607, L5

Ferrarese, L., & Merritt, D. 2000, ApJ, 539, L9

Ferrarese, L., et al. 2006, ApJ, 644, L21

Filippenko, A. V., & Sargent, W. L. W. 1989, ApJ, 342, L11

Gallo, E., Treu, T., Jacob, J., Woo, J.-H., Marshall, P., & Antonucci, R. 2007, ArXiv e-prints, 711, arXiv:0711.2073

Gebhardt, K., et al. 2000, ApJ, 539, L13

Gebhardt, K., et al. 2001, AJ, 122, 2469

Georgakakis, A., et al. 2008, arXiv0801.2160

Ghosh, H., Mathur, S., Fiore, F., & Ferrarese, L. 2008, ArXiv e-prints, 801, arXiv:0801.4382

Greene, J. E., & Ho, L. C. 2004, ApJ, 610, 722

Greene, J. E., & Ho, L. C. 2007, ApJ, 667, 131

Greene, J. E., & Ho, L. C. 2007, ApJ, 670, 92

Häring, N., & Rix, H.-W. 2004, ApJ, 604, L89

Heckman, T. M., Kauffmann, G., Brinchmann, J., Charlot, S., Tremonti, C., & White, S. D. M. 2004, ApJ, 613, 109

Heckman, T. M., Ptak, A., Hornschemeier, A., & Kauffmann, G. 2005, ApJ, 634, 161

Ho, L. C., Filippenko, A. V., & Sargent, W. L. 1995, ApJS, 98, 477

Ho, L. C., Filippenko, A. V., & Sargent, W. L. W. 1997, ApJ, 487, 568

Ho, L. C. 2008, ArXiv e-prints, 803, arXiv:0803.2268

Iovino, A., et al. 2005, A&A, 442, 423

Kauffmann, G., et al. 2003, MNRAS, 346, 1055

Kauffmann, G., et al. 2003, MNRAS, 341, 54

Kauffmann, G., et al. 2003, MNRAS, 341, 33

Kormendy, J., & Richstone, D. 1995, ARA&A, 33, 581

Laine, S., van der Marel, R. P., Lauer, T. R., Postman, M., O'Dea, C. P., & Owen, F. N. 2003, AJ, 125, 478

Laird, E. S., et al. 2008, ArXiv e-prints, 809, arXiv:0809.1349

Le Fèvre, O., et al. 2004, A&A, 417, 839

Le Fèvre, O., et al. 2005, A&A, 439, 845

Lodato, G., & Natarajan, P. 2006, MNRAS, 371, 1813

Lotz, J. M., et al. 2008, ApJ, 672, 177

Madau, P., & Rees, M. J. 2001, ApJ, 551, L27

Maiolino, R., & Rieke, G. H. 1995, ApJ, 454, 95

Magorrian, J., et al. 1998, AJ, 115, 2285

Marconi, A., Risaliti, G., Gilli, R., Hunt, L. K., Maiolino, R., & Salvati, M. 2004, MNRAS, 351, 169

McCracken, H. J., et al. 2003, A&A, 410, 17

McNamara, B. R., & Nulsen, P. E. J. 2007, ARA&A, 45, 117

Merritt, D., Ferrarese, L., & Joseph, C. L. 2001, Science, 293, 1116

Merritt, D., Milosavljević, M., Favata, M., Hughes, S. A., & Holz, D. E. 2004, ApJ, 607, L9

Nandra, K., et al. 2005, MNRAS, 356, 568

Nandra, K., et al. 2007, ApJ, 660, L11

Pérez-González, P. G., et al. 2008, ApJ, 675, 234

Radovich, M., et al. 2004, A&A, 417, 51

Ranalli, P., Comastri, A., & Setti, G. 2003, A&A, 399, 39

Risaliti, G., Maiolino, R., & Salvati, M. 1999, ApJ, 522, 157

Rossa, J., van der Marel, R. P., Böker, T., Gerssen, J., Ho, L. C., Rix, H.-W., Shields, J. C., & Walcher, C.-J. 2006, AJ, 132, 1074

Satyapal, S., Vega, D., Heckman, T., O'Halloran, B., & Dudik, R. 2007, ApJ, 663, L9

Satyapal, S., Vega, D., Dudik, R. P., Abel, N. P., & Heckman, T. 2008, ApJ, 677, 926

Schmidt, M. 1968, ApJ, 151, 393

Shankar, F., Salucci, P., Granato, G. L., De Zotti, G., & Danese, L. 2004, MNRAS, 354, 1020

Shi, Y., Rieke, G. H., Papovich, C., Pérez-González, P. G., & Le Floc'h, E. 2006, ApJ, 645, 199

Shields, J. C., Walcher, C. J., Boeker, T., Ho, L. C., Rix, H.-W., & van der Marel, R. P. 2008, ArXiv e-prints, 804, arXiv:0804.4024

Sivakoff, G. R., Martini, P., Zabludoff, A. I., Kelson, D. D., & Mulchaey, J. S. 2008, ArXiv e-prints, 804, arXiv:0804.3797

Steffen, A. T., Barger, A. J., Capak, P., Cowie, L. L., Mushotzky, R. F., & Yang, Y. 2004, AJ, 128, 1483

Szokoly, G. P., et al. 2004, ApJS, 155, 271

Valluri, M., Ferrarese, L., Merritt, D., & Joseph, C. L. 2005, ApJ, 628, 137
Verolme, E. K., et al. 2002, MNRAS, 335, 517
Volonteri, M., Lodato, G., & Natarajan, P. 2008, MNRAS, 383, 1079
Wehner, E. H., & Harris, W. E. 2006, ApJ, 644, L17
Willmer, C. N. A., et al. 2006, ApJ, 647, 853
Wolf, C., et al. 2004, A&A, 421, 913
Yang, Y., Mushotzky, R. F., Steffen, A. T., Barger, A. J., & Cowie, L. L. 2004, AJ, 128, 1501
Zakamska, N. L., et al. 2006, AJ, 132, 1496
Zezas, A. L., Georgantopoulos, I., & Ward, M. J. 1998, MNRAS, 301, 915

TABLE 1
X-ray Fields

FIELD (1)	Area deg^2 (2)	$F_{\mathrm{Xray}}^{\mathrm{limit}}$ erg s^{-1} cm^{-2} (3)	Ref (4)	Optical photometry (5)	Ref (6)	Secure redshift (7)	Ref (8)
AEGIS	0.67	5.0×10^{-16}	1	B, R, I, K$_s$	2,3	zquality=3, 4	4
CDF-N	0.12	1.4×10^{-16}	5	U, B, V, R, I, z, HK	6	all z without label $'$s$'$	6, 7
CDF-S	0.11	2.8×10^{-16}	8	U, B, V, R, I, 914nm	9	qual=2	10
CLASXS	0.4	3.0×10^{-15}	11	B, V, R, I, $z^{'}$	12	all listed z are secure	12
XMMLSS	1	5.8×10^{-15}	13	B, V, R, I, J, K	14,15,16,17	q$_{-}$z=3, 4, 13, 14, 23, 24	18

Note. — Col.(1): The field name. Col.(2): The area of the field size in square degree. Col.(3): The limiting X-ray flux in 2-8 keV. Col.(4): The reference for the X-ray data. Col.(5): The available optical/near-IR photometry. Col.(6): The reference for the optical/near-IR photometry. Col.(7): The definition of the secure spectroscopic redshift in each field. Col.(8): The reference for the spectroscopic redshift.

References – (1) Nandra et al. (2005); Laird et al. (2008); (2) Coil et al. (2004); (3) Bundy et al. (2006); (4) Davis et al. (2003, 2007); (5) Alexander et al. (2003); (6) Barger et al. (2003); (7) Barger et al. (2002); (8) Alexander et al. (2003); (9) Wolf et al. (2004) ; (10) Szokoly et al. (2004); (11) Yang et al. (2004); (12) Steffen et al. (2004); (13) Chiappetti et al. (2005); (14) Le Fèvre et al. (2004); (15) McCracken et al. (2003); (16) Radovich et al. (2004); (17) Iovino et al. (2005); (18) Le Fèvre et al. (2005)

TABLE 2
The number of X-ray objects in all fields

FIELD	CDF-N	CDF-S	CLASXS	AEGIS	XMMLSS
Total	503	326	525	1318	286
Spec-Observed	439	210	422	357	23

TABLE 3
The Parameters of Stellar Synthesis Models.

parameters	value
Simple stellar populations	Chabrier (2003) IMF and Padova 1994 evolutionary tracks
Metallicity	0.0001, 0.0004, 0.004, 0.008, 0.02 ($Z_{\odot}$), 0.05
visual extinction τ_v	[0.0, 4.0] with a step of 0.5 in logarithm
e-folding time τ for exponential star-formation history	[0.05, 8.91] Gyr with a step of 0.25 in logarithm, 100 Gyr
fraction of ejected gas to be recycled ϵ	0.001, 0.01, 0.1, 1
galaxy age	[0.001, 15.85] Gyr with a step of 0.1 in logarithm

TABLE 4
SAMPLE OF AGNS IN LOW-MASS HOST GALAXIES

source (1)	z (2)	$\mathrm{RA_X}$, $\mathrm{DEC_X}$ (3)	D_{opt} $['']$ (4)	Phtometry [in AB system] (5)	f_{X} $[10^{-15}\mathrm{ergs^{-1}cm^{-2}}]$ (6)	log(Mass) $[\log(\mathrm{M_\odot})]$ (7)	$f_{\mathrm{X}}/f_{\mathrm{r}}$ (8)
AEGIS123	0.92	14 15 39.2 +52 08 49.6	0.98	24.35, 23.95, 23.71, –	2.88	$9.52^{+0.40}_{-0.25}$	1.46
AEGIS232	0.81	14 16 16.8 +52 21 35.6	1.37	24.00, 23.31, 22.60, 21.62	1.06	$10.05^{+0.08}_{-0.07}$	0.32
AEGIS375	0.48	14 17 24.6 +52 30 25.0	0.31	20.23, 19.99, 19.66, 18.51	19.1	$10.21^{+0.07}_{-0.03}$	0.33
AEGIS555	0.84	14 18 25.2 +52 49 20.8	0.77	24.48, 24.06, 23.38, –	2.14	$9.64^{+0.15}_{-0.13}$	1.26
AEGIS655	0.71	14 19 06.5 +52 38 55.8	1.29	23.52, 22.65, 22.18, 20.93	3.26	$10.09^{+0.04}_{-0.08}$	0.56
AEGIS723	0.66	14 19 30.8 +52 56 17.3	0.42	25.99, 23.74, 22.76, 21.76	5.26	$10.25^{+0.35}_{-0.19}$	2.54
AEGIS795	0.46	14 20 01.4 +52 53 10.7	0.96	23.85, 21.91, 21.32, 20.16	2.40	$10.22^{+0.08}_{-0.01}$	0.25
AEGIS969	0.91	14 20 59.8 +52 56 04.3	0.92	23.06, 22.71, 22.00, 20.62	2.28	$10.06^{+0.00}_{-0.00}$	0.37
AEGIS1008	0.43	14 21 15.9 +53 19 48.6	0.38	22.27, 21.23, 20.81, 20.15	3.15	$9.92^{+0.31}_{-0.01}$	0.18
AEGIS1159	1.24	14 22 14.8 +53 23 54.3	1.90	24.02, 23.94, 23.35, –	1.55	$10.12^{+0.30}_{-0.25}$	0.67
AEGIS1303	1.00	14 23 26.1 +53 30 03.7	0.79	22.54, 21.89, 21.64, 20.69	11.4	$10.23^{+0.06}_{-0.01}$	0.84
CDF-N5	0.56	12 35 21.3 +62 16 28.1	0.05	23.20, 22.82, 22.42, 21.83, 21.35, 21.20, 20.59	4.22	$10.20^{+0.23}_{-0.33}$	0.37
CDF-N83	0.46	12 36 08.2 +62 15 53.1	1.52	23.50, 23.22, 22.62, 21.93, 21.55, 21.50, 20.89	3.52	$10.02^{+0.11}_{-0.11}$	0.37
CDF-N191	0.56	12 36 35.9 +62 07 07.7	1.43	25.40, 25.52, 25.22, 24.43, 23.85, 23.60, 21.59	5.31	$9.93^{+0.00}_{-0.00}$	5.15
CDF-N194	0.56	12 36 36.7 +62 11 56.0	0.34	24.30, 23.42, 23.12, 22.43, 21.85, 21.60, 20.80	2.01	$10.12^{+0.36}_{-0.26}$	0.31
CDF-N267	0.40	12 36 51.7 +62 12 21.4	0.97	24.20, 23.52, 22.62, 22.03, 21.65, 21.40, 20.59	2.65	$10.11^{+0.10}_{-0.13}$	0.31
CDF-N301	0.29	12 36 58.7 +62 04 02.4	0.62	22.20, 21.52, 21.62, 21.63, 21.65, 21.40, 21.09	5.69	$8.66^{+0.07}_{-0.15}$	0.51
CDF-N441	0.63	12 37 36.0 +62 18 05.9	0.00	25.20, 25.02, 24.52, 23.93, 23.45, 23.20, 21.59	1.12	$10.22^{+0.01}_{-0.05}$	0.65
CDF-S241	0.68	03 32 39.1 -27 44 39.1	1.62	25.84, 25.32, 25.44, 25.35, 24.54, 24.39	2.14	$8.35^{+0.37}_{-0.28}$	4.49
CLASXS42	0.49	10 31 54.9 +57 45 20.9	0.69	24.90, 24.70, 24.10, 24.20, 23.80	13.0	$8.63^{+0.14}_{-0.11}$	9.77
CLASXS131	0.39	10 32 42.6 +57 56 20.8	0.72	23.30, 23.90, 23.50, 23.10, 23.00	5.30	$8.89^{+0.16}_{-0.17}$	2.45
CLASXS205	0.68	10 33 18.1 +57 26 01.4	0.65	21.50, 22.00, 21.70, 21.40, 21.10	22.0	$9.43^{+0.02}_{-0.29}$	1.60
CLASXS231	1.38	10 33 29.2 +57 47 08.1	0.56	23.40, 23.60, 23.20, 23.30, 23.30	5.90	$10.15^{+0.24}_{-0.31}$	1.21
CLASXS243	0.32	10 33 34.1 +57 56 01.9	0.18	21.90, 21.20, 20.50, 20.20, 19.80	8.20	$10.08^{+0.20}_{-0.32}$	0.25
CLASXS286	0.29	10 33 53.2 +57 32 41.0	0.48	21.00, 20.90, 20.20, 20.00, 19.60	14.0	$9.61^{+0.06}_{-0.29}$	0.33
CLASXS322	0.20	10 34 06.6 +57 56 07.3	0.26	21.50, 21.00, 20.50, 20.20, 19.90	19.0	$9.59^{+0.19}_{-0.53}$	0.64
CLASXS329	0.37	10 34 09.5 +57 29 53.8	0.30	22.60, 21.80, 21.20, 21.00, 20.60	5.40	$10.19^{+0.12}_{-0.11}$	0.31
CLASXS373	0.33	10 34 29.7 +57 50 58.2	0.69	22.70, 22.00, 21.20, 20.80, 20.30	9.80	$10.07^{+0.06}_{-0.32}$	0.57
CLASXS441	0.39	10 34 56.2 +57 47 24.5	0.85	23.90, 23.00, 22.10, 21.70, 21.20	20.0	$10.26^{+0.22}_{-0.38}$	2.55
CLASXS448	0.62	10 34 57.9 +57 37 56.1	0.42	25.30, 24.70, 23.90, 23.00, 22.90	13.0	$10.22^{+0.13}_{-0.17}$	7.49
CLASXS517	0.62	10 35 51.0 +57 43 33.0	0.28	21.10, 21.10, 20.90, 20.50, 20.20	73.0	$9.92^{+0.04}_{-0.03}$	2.65
CLASXS522	0.51	10 36 04.2 +57 47 48.3	0.17	23.60, 23.20, 22.50, 22.20, 21.70	1.90	$9.74^{+0.36}_{-0.34}$	0.32

NOTE. — Col.(1): Source name. Col.(2): Redshift. Col.(3): RA and DEC of the X-ray target. Col.(4): The distance in arcsec of the optical counterpart from the X-ray target. Col.(5): Optical/near-IR photometry in AB system. The photometric bands for each field are listed in Table 1. Col.(6): The observed-frame 2-8 KeV X-ray flux. Col.(7): The stellar mass. Col.(8): The hard X-ray to *R*-band flux ratio.